Journal of Quality Measurement and Analysis *JQMA* 22(2) 2026, 137-155
e-ISSN: 2600-8602 *http://www.ukm.my/jqma*
https://doi.org/10.17576/jqma.2022.2026.08

DESIGN OF THE MULTIVARIATE SIDE-SENSITIVE SYNTHETIC COEFFICIENT OF VARIATION CHART BASED ON THE MEDIAN RUN LENGTH

(*Rekaan Carta Multivariat Sintetik Peka Arah untuk Pekali Variasi Berdasarkan Panjang Larian Median*)

WAI CHUNG YEONG*, SOK LI LIM, NURUL SHUHADA BINTI SHAMSUN NUR, ZHI LIN CHONG & PEH SANG NG

ABSTRACT

The multivariate side-sensitive synthetic chart shows good detection capabilities for shifts in the coefficient of variation (γ); however, its design and evaluation is dependent on the average run length (*ARL*), which fairly represents its performance only for symmetrically distributed run lengths, and a skewed run length will result in an actual performance that frequently differs from its *ARL*, resulting in a loss of trust for the chart. Through numerical analysis, this paper has shown that the in-control run length and out-of-control run length of small shift sizes (τ) has a right-skewed distribution, showing that the chart could not be evaluated based on only its *ARL*. Following this finding, a design building upon the median run length (*MRL*) is proposed. This design resulted in a smaller out-of-control *MRL* (MRL_1) than the design based on its *ARL*. Hence, the design shows faster detection and presents a more accurate representation of the chart's performance. A design based on the expected *MRL* (*EMRL*) was also proposed for practitioners who are unable to estimate the exact value for τ . The proposed designs are also implemented in a real-life application monitoring investment risk.

Keywords: average run length; coefficient of variation; median run length; percentiles of the run length; side-sensitive synthetic chart

ABSTRAK

Carta multivariat sintetik peka arah menunjukkan pengesanan yang baik untuk perubahan dalam pekali variasi; namun begitu, reka bentuk dan penilaiannya adalah berdasarkan panjang larian purata (*PLP*), yang hanya memberikan gambaran yang tepat terhadap prestasi carta apabila panjang larian adalah bertaburan secara simetri, dan panjang larian yang bertaburan condong akan menyebabkan prestasi sebenar sering berbeza daripada *PLP*, sekali gus menimbulkan kekurangan keyakinan terhadap carta tersebut. Melalui analisis berangka, kajian ini menunjukkan bahawa panjang larian dalam kawalan dan luar kawalan bagi saiz perubahan (τ) yang kecil mempunyai taburan condong ke kanan, menunjukkan bahawa carta tidak seharusnya dinilai berdasarkan *PLP* sahaja. Berikutan penemuan ini, reka bentuk carta berdasarkan panjang larian median (*PLM*) telah dicadangkan. Reka bentuk ini menghasilkan PLM luar kawalan (PLM_1) yang lebih kecil berbanding reka bentuk berdasarkan *PPL*. Oleh itu, reka bentuk ini menunjukkan pengesanan keadaan luar kawalan yang lebih pantas dan memberikan gambaran yang lebih tepat terhadap prestasi carta. Satu reka bentuk berdasarkan jangkaan *PLM* (*JPLM*) juga dicadangkan untuk pengamal yang tidak dapat menganggar nilai sebenar bagi τ . Reka bentuk yang dicadangkan juga dilaksanakan dalam aplikasi sebenar yang memantau risiko pelaburan.

Kata kunci: carta sintetik peka arah; panjang larian median; panjang larian purata; pekali variasi; peratusan panjang larian

1. Introduction

Control charts are tools that are frequently adopted in industries to monitor process stability, by signalling to the user whenever there are shifts in some statistical parameters, which can include the mean, standard deviation, proportion or coefficient of variation (γ). Charts monitoring γ are increasingly receiving attention in the literature due to its capabilities in monitoring processes with inconsistent mean and standard deviation that varies according to its mean. A review of the various studies available for γ charts is available from Jalilibal *et al*. (2021).

Control charts monitoring γ for multivariate processes was initiated by Yeong *et al.* (2016). Unlike univariate charts, correlations between multiple quality characteristics are taken into consideration in Yeong *et al.* (2016). Multiple new charts with better sensitivity in detecting shifts in γ for multivariate processes are then proposed, for example Lim *et al.* (2017) developed a run sum chart; Abbasi and Adegoke (2018) proposed charts for better estimation of control limits; Khatun *et al*. (2018) developed charts for short production runs; Khaw *et al.* (2018) proposed charts with variable sample sizes and intervals, which was extended by Chew *et al.* (2019) who varied the chart's limits followed by Sabahno and Celano (2023) who considers autocorrelation; Giner-Bosch *et al*. (2019) proposed an exponentially weighted moving average (EWMA) chart, which was extended by Haq and Khoo (2022) for individual observations; Chew *et al.* (2020) developed run rules charts, which was extended for short production runs by Chew *et al*. (2022); Ayyoub *et al.* (2020) proposed charts for measurement errors; Adegoke *et al.* (2022) proposed charts for high dimensional processes with small sample sizes; and finally Hu *et al.* (2023) proposed a cumulative sum (CUSUM) chart.

A synthetic chart for multivariate γ was developed by Khaw *et al*. (2019), where a sample γ $(\hat{\gamma})$ falling outside control limits does not trigger out-of-control signals, instead it waits for a second $\hat{\gamma}$ that is outside the limits, during which the chart counts the number of samples between these two $\hat{\gamma}$. With counts less than a threshold, out-of-control signals are produced. Yeong *et al*. (2022) then developed a side-sensitive version, where successive $\hat{\gamma}$ that falls outside the control limits should fall on the same side of its control limits (*CL*). As an example, when a $\hat{\gamma}$ is above the upper control limit (*UCL*), then the number of samples until a second $\hat{\gamma}$ to fall above the *UCL* is considered. Similarly when $\hat{\gamma}$ is below the lower control limit (*LCL*). This feature improves the synthetic chart's performance (Yeong *et al.* 2022).

The charts from the preceding paragraph are evaluated through their *ARL*, measuring the average number of samples until the chart produces out-of-control signals. The *ARL* is categorised as the in-control and out-of-control *ARL* (ARL_0 and ARL_1). The ARL_0 looks at the average number of samples until the occurrence of a false alarm. Conversely, ARL_1 measures the average number of samples before the out-of-control assignable cause(s) are detected. Conventionally, charts are designed to minimise their ARL_1 while fulfilling constraints in ARL_0.

The *ARL* is a good measure of performance if its run length (i.e. the number of samples to produce an out-of-control signal) is symmetrically distributed, however, numerous studies have shown that the in-control run length and out-of-control run length of small shifts is right-skewed and not symmetrical. Among univariate γ charts, Teoh *et al*. (2019), Lim *et al.* (2019), Yeong *et al*. (2021a) and Yeong *et al*. (2021b) studied the run length's skewness for the EWMA, variable sample size (VSS), synthetic and side-sensitive synthetic charts, respectively, while for the multivariate γ charts, Lee *et al*. (2020) and Karimi *et al*. (2023) have studied the skewness for the synthetic and VSS charts, respectively. In these studies, the ARL_0 was found to be larger than the typical in-control run length, while the ARL_1 for small shift sizes was found to be larger than the typical out-of-control run lengths. Hence, the *ARL* might not be an accurate representation of the chart's performance. These studies then design the charts with its median run length (*MRL*).

Although studies on the run length's skewness are available for several charts, it is not available for the multivariate side-sensitive synthetic γ chart. Hence, this gap will be filled. Studies on the run length's skewness based on the chart's existing design are conducted. Subsequently, the chart is designed with its *MRL*. As the design based on the *MRL* requires the exact value of τ, this paper also designs the chart based on its expected *MRL* (*EMRL*), which only requires τ to be estimated as a range.

The paper is organised as follows. The next section shows the lists of abbreviations and notations used throughout the paper, followed by Section 3 which reviews properties of the sample γ $(\hat{\gamma})$. Subsequently, Section 4 first reviews the operations for the chart and the computation of its *ARL*, followed by the proposal of the *MRL*-based and *EMRL*-based designs. Section 5 then presents the numerical results and analysis, followed by the implementation of the proposed design on a real-life example in Section 6. Conclusions are then made in Section 7.

2. List of Abbreviations and Notations

Table 1 presents the list of abbreviations and notations used throughout the paper.

Table 1: List of abbreviations and notations

Abbreviations/ notations	Description	Abbreviations/ notations	Description
ARL	Average run length	Q_{05}	5th run length percentile
ARL_0	In-control *ARL*	Q_{95}	95th run length percentile
ARL_1	Out-of-control *ARL*	EQ_{05}	5th expected run length percentile
MRL	Median run length	EQ_{95}	95th expected run length percentile
MRL_0	In-control *MRL*	τ	Shift size
MRL_1	Out-of-control *MRL*	γ	Coefficient of variation
EMRL	Expected median run length	$\hat{\gamma}$	Sample γ
CL	Control limits	γ_0	In-control γ
UCL	Upper control limit	γ_1	Out-of-control γ
LCL	Lower control limit	$f_\tau(\tau)$	Pdf of τ
CRL	Conforming run length	$\boldsymbol{\mu}$	Mean vector
VSS	Variable sample size	$\boldsymbol{\Sigma}$	Covariance matrix
cdf	Cumulative distribution function	$\bar{\mathbf{X}}$	Sample mean vector
pdf	Probablity density function	$\mathbf{S}$	Sample covariance matrix
n	Sample size	$\mathbf{q}$	Initial probability vector
p	Number of variables	$\mathbf{I}$	Identity matrix
K	Control limit coefficient	$\mathbf{1}$	Vector of ones
L	Threshold for CRL	$\mathbf{Q}$	Transition probability matrix

3. Properties of the Sample Multivariate Coefficient of Variation ($\hat{\gamma}$)

Suppose $\mathbf{X}$ is a p-variate quality characteristic as follows:

$$\mathbf{X}=\begin{pmatrix} X_{11} & \cdots & X_{n1} \\ \vdots & \ddots & \vdots \\ X_{1p} & \cdots & X_{np} \end{pmatrix}=\left(\mathbf{X}_1,\ldots,\mathbf{X}_n\right), \tag{1}$$

where X_{ij} represents the i^{th} observation for the j^{th} variable, with $i=1,...,n$ and $j=1,...,p$, while $\mathbf{X}_i, i=1,...,n$ represents the i^{th} observation of $\mathbf{X}$. Note that n is the sample size while p is the number of variables. Assumed $\mathbf{X}\sim N(\boldsymbol{\mu},\boldsymbol{\Sigma})$, with $\boldsymbol{\mu}$ being the mean vector consisting of the means for the $j=1,...,p$ variables, while $\boldsymbol{\Sigma}$ is the covariance matrix. The multivariate γ is:

$$\gamma=\left(\boldsymbol{\mu}^T\boldsymbol{\Sigma}^{-1}\boldsymbol{\mu}\right)^{-\frac{1}{2}}, \tag{2}$$

while $\hat{\gamma}$ is computed as:

$$\hat{\gamma}=\left(\bar{\mathbf{X}}^T\mathbf{S}^{-1}\bar{\mathbf{X}}\right)^{-\frac{1}{2}}, \tag{3}$$

where $\bar{\mathbf{X}}$ is the sample mean vector obtained by averaging each row of $\mathbf{X}$ in Eq. (1), i.e.,

$$\bar{\mathbf{X}}=\left(\frac{1}{n}\sum_{i=1}^{n}X_{i1},\ldots,\frac{1}{n}\sum_{i=1}^{n}X_{ip}\right)^T, \tag{4}$$

while $\mathbf{S}$ is the sample covariance matrix given by

$$\mathbf{S}=\frac{1}{n-1}\sum_{i=1}^{n}\left(\mathbf{X}_i-\bar{\mathbf{X}}\right)\left(\mathbf{X}_i-\bar{\mathbf{X}}\right)^T, \tag{5}$$

where $\mathbf{X}_i$ denotes the i^{th} observation of $\mathbf{X}$ as shown in Eq. (1).

The cumulative distribution function (cdf) for $\hat{\gamma}^2$ is (Yeong *et al*. 2016)

$$F_{\hat{\gamma}^2}\left(x\middle|n,p,\gamma\right)=1-F_F\left(\frac{n(n-p)}{(n-1)px}\middle|p,n-p,\frac{n}{\gamma^2}\right), \tag{6}$$

where $F_F\left(.\middle|p,n-p,\frac{n}{\gamma^2}\right)$ denotes the cdf for the non-central *F* distribution with p and $n-p$ degrees of freedom and non-centrality parameter $\frac{n}{\gamma^2}$. As the *F* distribution is well-known for its sensitivity towards non-normal data, the results in this paper may not be applicable for non-normal variables.

4. Multivariate Side-sensitive Synthetic γ Chart

The section is made up of two sub-sections. Firstly, this chart is reviewed, followed by the second section, which shows the new design based on the *MRL*.

4.1. *Review of the multivariate side-sensitive synthetic γ chart*

Procedures for implementing the chart are illustrated as follows:

(i) Determine the values for *n*, *p*, the in-control γ (γ_0) and compute the *LCL* and *UCL* as follows:

$$LCL = \mu_0\left(\hat{\gamma}^2\right) - K\sigma_0\left(\hat{\gamma}^2\right) \tag{7}$$

and

$$UCL = \mu_0\left(\hat{\gamma}^2\right) + K\sigma_0\left(\hat{\gamma}^2\right), \tag{8}$$

where *K* denotes the control limit coefficient that needs to be determined by the user, while $\mu_0(\hat{\gamma}^2)$ and $\sigma_0\left(\hat{\gamma}^2\right)$ are obtained through the methodology described in Giner-Bosch *et al*. (2019), by letting $\gamma = \gamma_0$. The value of *K* is determined to control the in-control run lengths so that the number of false alarms are controlled. For designs based on the *ARL*, it is determined to satisfy ARL_0 constraints, whereas for designs based on the *MRL*, it is determined to satisfy in-control *MRL* (MRL_0) constraints.

(ii) Initialise the conforming run length (CRL) as 0 and go to Step (iii).

(iii) A sample of n items is collected, and $\hat{\gamma}$ is computed from Eq. (3).

Add 1 to the CRL.

If $LCL < \hat{\gamma} < UCL$, the sample conforms and this step is repeated;

conversely if $\hat{\gamma} > UCL$, it is an upper non-conforming sample and proceed to Step (iv);

while if $\hat{\gamma} < LCL$, it is a lower non-conforming sample and proceed to Step (v).

(iv) If this is the first $\hat{\gamma}$ above the UCL, go to Step (viii), else go to Step (vi).

(v) If this is the first $\hat{\gamma}$ below the LCL, go to Step (viii), else go to Step (vii).

(vi) Count the number of samples between the most recent sample that is above the UCL and the current sample, inclusive of the current sample. Define it as the CRL and go to Step (viii).

(vii) Count the number of samples between the most recent sample that is below the LCL and the current sample, inclusive of the current sample. Define it as the CRL and go to Step (viii).

(viii) If $CRL \le L$, where L is a pre-determined threshold, then an out-of-control signal is issued; conversely go back to Step (ii).

Figure 1 shows a graphical representation of how the CRL is obtained. From Figure 1, Sample 2 is the first sample to fall above the *UCL*. As it is the first non-conforming sample, the CRL will be computed, where $\mathrm{CRL}_1 = 2$. An out-of-control signal will be produced as *L* must be at least 2. Next, Sample 5 is below the *LCL*. However, the CRL is not computed as the most recent non-conforming sample (Sample 2) is above the *UCL*. The CRL is only computed when Sample 7 falls above the *UCL*, where the CRL = 5. An out-of-control signal will be issued for any $L \geq 5$, whereas the process is considered in-control for $L < 5$.

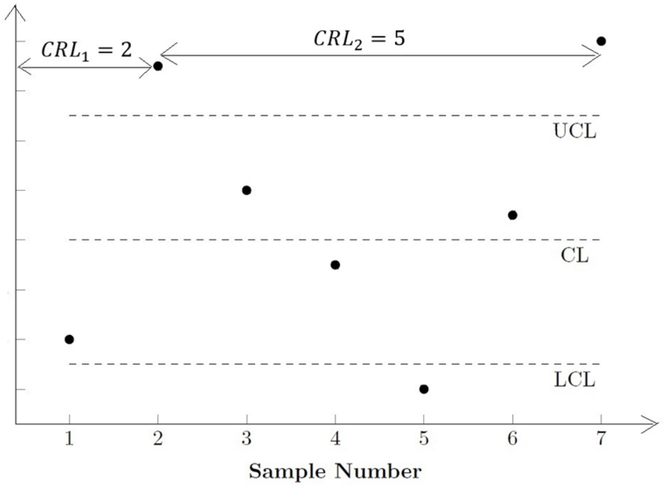

Figure 1: CRL computation

To obtain the optimal (L, K), Yeong *et al*. (2022) select the combination that minimises the ARL_1, subject to constraints in the ARL_0. A Markov chain approach is adopted, where the states are defined based on a string of L successive samples, where each sample is either between the *LCL* and *UCL* (0), below the *LCL* ($\underline{1}$) or above the *UCL* (1). The following are the states of the Markov chain:

State 1 : $\underline{1}$00..0
State 2 : 0$\underline{1}$0..0
State 3 : 00$\underline{1}$..0
⋮
State L : 000..$\underline{1}$
State $L + 1$: 00..00
State $L + 2$: 0..001
State $L + 3$: 0..010
⋮
State $2L$: 010..0
State $2L + 1$: 100..0
State $2L + 2$: Signaling state (i.e., the state where the chart signals an out-of-control condition when $CRL \leq L$)

Yeong *et al*. (2022) then formed a $(2L+2)\times(2L+2)$ transition probability matrix as follows:

$$\mathbf{P}=\begin{pmatrix}\mathbf{Q} & \mathbf{r}\\ \mathbf{0}^T & 1\end{pmatrix}=\begin{array}{c} \\ 1\\ 2\\ 3\\ \vdots\\ L\\ L+1\\ L+2\\ L+3\\ \vdots\\ 2L\\ 2L+1\\ 2L+2\end{array}\begin{array}{c}\begin{array}{cccccccccccc}1 & 2 & \cdots & L-1 & L & L+1 & L+2 & L+3 & L+4 & \cdots & 2L+1 & 2L+2\end{array}\\ \begin{pmatrix}0 & 0 & \cdots & 0 & 0 & A & B^+ & 0 & 0 & \cdots & 0 & B^-\\ A & 0 & \cdots & 0 & 0 & 0 & B^+ & 0 & 0 & \cdots & 0 & B^-\\ 0 & A & \cdots & 0 & 0 & 0 & B^+ & 0 & 0 & \cdots & \cdots & B^-\\ \cdots & \cdots & \cdots & \cdots & \cdots & \cdots & \cdots & \cdots & \cdots & \cdots & \cdots & \cdots\\ 0 & 0 & \cdots & A & 0 & 0 & B^+ & 0 & 0 & \cdots & 0 & B^-\\ 0 & 0 & \cdots & 0 & B^- & A & B^+ & 0 & 0 & \cdots & 0 & 0\\ 0 & 0 & \cdots & 0 & B^- & 0 & 0 & A & 0 & \cdots & 0 & B^+\\ 0 & 0 & \cdots & 0 & B^- & 0 & 0 & 0 & A & \cdots & 0 & B^+\\ \cdots & \cdots & \cdots & \cdots & \cdots & \cdots & \cdots & \cdots & \cdots & \cdots & \cdots & \cdots\\ 0 & 0 & \cdots & 0 & B^- & 0 & 0 & 0 & 0 & \cdots & A & B^+\\ 0 & 0 & \cdots & 0 & B^- & A & 0 & 0 & 0 & \cdots & 0 & B^+\\ 0 & 0 & \cdots & 0 & 0 & 0 & 0 & 0 & 0 & \cdots & 0 & 1\end{pmatrix}\end{array}, \tag{9}$$

where A, B^+ and B^- are the probabilities $P\left(LCL < \hat{\gamma}^2 < UCL\right)$, $P\left(\hat{\gamma}^2 > UCL\right)$ and $P\left(\hat{\gamma} < LCL\right)$, respectively, and can be computed from Eq. (6). The *ARL* is then obtained as

$$ARL = \mathbf{q}^T \left(\mathbf{I}-\mathbf{Q}\right)^{-1}\mathbf{1}, \tag{10}$$

where $\mathbf{q}$ is a $(2L+1)\times 1$ vector with the $(L+2)^{\text{th}}$ element being one and the remaining elements being zeros, $\mathbf{I}$ is the identity matrix, $\mathbf{1}$ is a vector of ones and $\mathbf{Q}$ is obtained from Eq. (9). The ARL_0 is obtained when $\gamma=\gamma_0$ in Eq. (10), while the ARL_1 is obtained when $\gamma=\gamma_1=\tau\gamma_0$, where γ_1 is the out-of-control γ. The algorithm to select the (L,K) combination minimising its ARL_1 with ARL_0 constraints is shown in Yeong *et al.* (2022).

4.2. *MRL-based and EMRL-based Designs*

This section presents the design where (L,K) is selected to minimise its out-of-control MRL (MRL_1), with constraints in its MRL_0. The MRL is the run length's 50$^{\text{th}}$ percentile, which can be obtained from the run length's cdf, $F_{RL}(l)$. $F_{RL}(l)$ is defined as follows:

$$F_{RL}(l) = P\left(RL \le l\right) = 1-\mathbf{q}^T\left(\mathbf{Q}^{l-1}\right)\mathbf{1}, \tag{11}$$

where $\mathbf{q}$, $\mathbf{Q}$ and $\mathbf{1}$ are as defined in Eq. (10). The $(100\theta)^{th}$ percentile is obtained by searching for l_θ such that

$$P\left(RL \le l_\theta - 1\right) \le \theta \text{ and } P\left(RL \le l_\theta\right) > \theta, \tag{12}$$

with $0<\theta<1$. Note that $\gamma=\gamma_0$ for in-control percentiles, while $\gamma=\gamma_1$ for the out-of-control percentiles. The optimal (L,K) are obtained through the following procedures:

(i) Determine the values for $n, p,\ \gamma_0$ and τ. Fix the value of the MRL_0 as ξ.
(ii) Set $L = 2$ as the initial value.
(iii) Numerically solve Eq. (12) for K when $l_{0.5}=\xi$ and $\gamma=\gamma_0$.

(iv) Numerically search for $l_{0.5}$ that satisfies Eq. (12) when $\gamma = \tau\gamma_0$. This $l_{0.5}$ is the *MRL*1.
(v) *L* is increased by 1.
(vi) Repeat Steps (iii) to (v) until the *MRL*1 of *L* + 1 exceeds that of *L*, after which the procedure is terminated and the optimal (L, K) is selected. If there are multiple combinations of (L, K) with the smallest *MRL*1, the combination with the smallest difference between $l_{0.05}$ and $l_{0.95}$ will be selected, where $l_{0.05}$ and $l_{0.95}$ are obtained from Eq. (12) by letting $\theta = 0.05$ and $\theta = 0.95$, respectively.

The above procedures are implemented by writing a program in Scicoslab, where the output can be obtained within a few minutes with a conventional computer. Although the design involves additional iterations to search for the run length percentiles through Equation (12), which is not required in the design based on the *ARL*, the additional search does not result in a noticeable increase in the computational time. Hence, the time required to obtain the output is similar to the *ARL*-based design in Section 4.1.

Procedures in Steps (i) to (vi) requires τ to be determined. The value of τ depends on the size of shift that the practitioner needs to detect. For example, if it is important for the practitioner to detect a 30% increase in γ_0, then the τ should be set as 1.3. The size of τ can be estimated from a set of historical out-of-control samples, where γ_1 can be obtained as the average $\hat{\gamma}$ of these samples. Note that $\tau = \frac{\gamma_1}{\gamma_0}$.

However, it is difficult in practice to estimate the exact value of τ as a result of insuffient historical out-of-control data. It is also possible for τ to be non-deterministic and vary according to unknown stochastic models (Castagliola *et al.* 2011). To resolve this issue, the expected percentiles of the run-length distribution, $E(l_\theta)$ are evaluated. $E(l_\theta)$ only requires τ to be specified as a range of possible values, $(\tau_{\min}, \tau_{\max})$, and is computed as follows:

$$E(l_\theta) = \int_{\tau_{\min}}^{\tau_{\max}} f_\tau(\tau) l_\theta(\tau) d\tau, \tag{13}$$

where $l_\theta(\tau)$ is obtained from Eq. (12) and $f_\tau(\tau)$ is the pdf of τ. If information regarding the actual distribution of τ is unknown, τ is assumed to be uniformly distributed, hence $f_\tau(\tau) = \frac{1}{\tau_{\max} - \tau_{\min}}$ (Castagliola *et al.* 2011). The integral in Eq. (13) can be approximated using the Gauss-Legendre quadrature through a built-in function in Scicoslab. Hence $E(l_\theta)$ actually approximates the weighted average of $l_\theta(\tau)$ over the range $(\tau_{\min}, \tau_{\max})$.

For cases where the exact value of τ could not be estimated, the optimal (L, K) can be obtained to minimise the expected median run length (*EMRL*) instead, where $EMRL = E(l_{0.5})$. The following procedures can be applied:

(i) Determine n, p, γ_0, $\tau_{\min}$ and $\tau_{\max}$. Fix the value of the *MRL*0 as ξ.
(ii) Set *L* = 2 as the initial value.
(iii) Numerically solve Eq. (12) for *K* when $l_{0.5} = \xi$ and $\gamma = \gamma_0$.

(iv) Numerically search for $E\left(l_{0.5}\right)$ that satisfies Eq. (13). This $E\left(l_{0.5}\right)$ is the *EMRL*.

(v) L is increased by 1.

(vi) Repeat Steps (iii) to (v) until the *EMRL* of L + 1 exceeds that of L, after which the procedure is terminated and the optimal $\left(L, K\right)$ is selected. If there are multiple combinations of $\left(L, K\right)$ with the smallest *EMRL*, the combination with the smallest difference between $E\left(l_{0.05}\right)$ and $E\left(l_{0.95}\right)$ will be selected, where $E\left(l_{0.05}\right)$ and $E\left(l_{0.95}\right)$ are obtained from Eq. (13) by letting $\theta = 0.05$ and $\theta = 0.95$, respectively.

5. Numerical Analysis

In this section, the distribution for the run lengths will be analysed through its percentiles, followed by studies on the optimal charting parameters from designs in Section 4.2. The following values are considered: $\gamma_0 = 0.10, p \in \{2,3,5,8\}, n \in \{5,6,10,15\}$ and $\tau \in \{1.1,1.2,1.3,1.5,2.0\}$.

Table 2 shows the optimal $\left(L, K\right)$ from the *ARL*-based design by Yeong *et al.* (2022), which satisfies the constraint $ARL_0 = 370.4$.

Table 2: Optimal charting parameters and the corresponding ARL_1 for the *ARL*-based design

τ	**p = 2**						**p = 3**					
	n = 5			n = 10			n = 5			n = 10		
	L	K	ARL_1	L	K	ARL_1	L	K	ARL_1	L	K	ARL_1
1.1	47	3.60	74.72	31	3.04	44.09	53	3.87	88.50	33	3.10	47.95
1.2	27	3.37	26.36	15	2.80	12.50	34	3.66	34.01	16	2.86	14.01
1.3	18	3.20	12.94	9	2.63	5.69	23	3.48	17.42	10	2.70	6.42
1.5	10	2.95	5.36	5	2.43	2.41	13	3.21	7.40	6	2.52	2.68
2.0	5	2.64	2.10	3	2.25	1.22	7	2.91	2.81	3	2.27	1.29
τ	p = 5						p = 8					
	n = 6			n = 10			n = 10			n = 15		
1.1	71	4.46	112.56	37	3.26	58.24	57	3.89	88.72	31	3.08	48.01
1.2	47	4.23	49.41	20	3.04	18.36	33	3.64	34.14	17	2.88	14.03
1.3	34	4.04	27.29	13	2.88	8.61	23	3.47	17.50	10	2.69	6.43
1.5	21	3.76	12.39	7	2.65	3.53	13	3.20	7.45	6	2.52	2.69
2.0	11	3.37	4.73	4	2.44	1.53	7	2.90	2.83	3	2.27	1.29

The *ARL* in Table 2 only shows the average of the run lengths. The actual run length distribution is not known with these values alone. For example, the actual run length may be very different from the *ARL* for a skewed run length. Hence, for a better understanding of the actual run length performance, its complete run length distribution is examined. The chart's 5th until 95th in-control percentiles are displayed in Table 3, and Table 4 displays its out-of-control percentiles. The in-control percentiles refer to percentiles of the in-control run length, where in-control run length represents the number of samples taken until the chart produces a false alarm. For example, an in-control 50th percentile of 207 shows that for 50 percent of the time, a false alarm will happen by the 207th sample. On the other hand, out-of-control percentiles refer to percentiles of the out-of-control run length, where out-of-control run length represents the number of samples taken until the chart detects the out-of-control condition. For example, an out-of-control 50th percentile of 33 for $\tau = 1.1$ shows that for 50 percent of the time, a shift size of 1.1 can the detected by the 33rd sample.

Table 3: In-control percentiles based on (L, K) in Table 2

τ	5th	10th	20th	30th	40th	50th	60th	70th	80th	90th	95th
						$p = 2, n = 5$					
1.1	7	13	27	43	121	207	313	449	640	968	1296
1.2	5	10	21	68	138	220	321	451	634	947	1259
1.3	4	9	18	80	148	228	326	452	631	935	1240
1.5	3	7	37	94	160	237	332	455	628	923	1218
2.0	3	5	50	104	166	240	330	447	611	892	1173
τ						$p = 2, n = 10$					
1.1	6	11	23	64	134	217	319	451	636	953	1270
1.2	4	8	26	84	150	229	325	449	623	922	1221
1.3	3	6	39	95	160	236	330	451	621	912	1203
1.5	3	5	50	105	169	244	335	453	620	905	1189
2.0	2	10	58	112	174	247	337	452	616	894	1173
τ						$p = 3, n = 5$					
1.1	7	14	29	46	118	205	312	450	645	978	1311
1.2	6	11	24	61	131	215	317	449	635	954	1272
1.3	5	10	20	74	143	225	325	454	636	947	1258
1.5	4	7	31	89	156	235	332	457	633	933	1234
2.0	3	6	45	101	165	242	335	456	626	917	1207
τ						$p = 3, n = 10$					
1.1	6	11	23	62	131	214	316	448	633	949	1266
1.2	4	8	23	83	150	230	327	452	629	931	1233
1.3	3	7	37	94	160	237	332	455	627	923	1218
1.5	3	5	47	103	167	242	335	454	622	910	1197
2.0	2	10	58	112	174	247	337	453	616	895	1174
τ						$p = 5, n = 6$					
1.1	8	16	33	52	99	193	302	442	640	979	1317
1.2	7	13	27	43	121	208	314	450	642	971	1300
1.3	6	11	24	61	131	215	318	451	637	957	1276
1.5	5	9	19	76	145	226	326	454	635	944	1254
2.0	4	7	34	91	156	234	328	450	622	917	1211
τ						$p = 5, n = 10$					
1.1	6	12	24	54	127	211	314	446	632	951	1269
1.2	5	9	18	76	144	225	323	449	628	933	1238
1.3	4	7	30	87	153	230	326	448	621	917	1213
1.5	3	6	44	100	164	239	332	452	620	908	1196
2.0	2	4	54	109	172	247	338	456	622	907	1191
τ						$p = 8, n = 10$					
1.1	7	14	30	47	116	202	310	449	644	979	1313
1.2	6	11	23	63	133	217	320	452	639	958	1277
1.3	5	10	20	73	142	223	323	452	633	943	1253
1.5	4	7	30	88	154	233	329	452	627	925	1224
2.0	3	6	44	99	163	238	331	450	617	904	1191
τ						$p = 8, n = 15$					
1.1	6	11	23	65	136	220	323	456	643	963	1283
1.2	4	8	17	83	151	231	330	457	637	943	1250
1.3	3	7	36	92	157	233	327	448	618	909	1199
1.5	3	5	48	104	168	244	338	458	627	917	1207
2.0	2	11	58	112	175	248	339	455	619	900	1180

From Table 3, the MRL_0 obtained is between 193 to 248, with a smaller MRL_0 being observed when n, p and τ are larger. A significant difference is shown with the ARL_0 of 370.4, indicating false alarms occuring far earlier than the 370th sample for 50% of the time. Practitioners would anticipate that false alarms would often occur by the 370th sample when designing the chart based on an ARL_0 of 370.4, which is frequently not the case from the MRL_0 in Table 2. This may result in a reduced trust in the chart. In fact, 370 is in the 60^{th} to 70^{th} percentile. This indicates that its in-control run length is right-skewed, making interpretations of its false alarm frequency through its ARL_0 inaccurate. Next, Table 4 presents its out-of-control percentiles.

Table 4: Out-of-control percentiles based on (L, K) in Table 2

	5^{th}	10^{th}	20^{th}	30^{th}	40^{th}	50^{th}	60^{th}	70^{th}	80^{th}	90^{th}	95^{th}
τ						$p = 2, n = 5$					
1.1	3	5	11	17	24	33	43	84	126	201	277
1.2	1	3	5	7	10	14	18	24	43	69	96
1.3	1	2	3	4	6	8	10	13	17	34	46
1.5	1	1	1	2	3	3	4	6	7	10	18
2.0	1	1	1	1	1	2	2	2	3	4	5
τ						$p = 2, n = 10$					
1.1	2	4	7	11	15	20	27	49	74	118	163
1.2	1	1	3	4	5	7	9	12	18	32	45
1.3	1	1	1	2	3	4	5	6	8	14	19
1.5	1	1	1	1	1	2	2	3	3	4	7
2.0	1	1	1	1	1	1	1	1	1	2	2
τ						$p = 3, n = 5$					
1.1	3	6	13	20	28	38	51	100	151	240	329
1.2	2	3	6	9	13	18	23	30	56	90	125
1.3	1	2	4	5	7	10	13	17	23	45	63
1.5	1	1	2	3	4	5	6	8	10	18	26
2.0	1	1	1	1	2	2	2	3	4	5	7
τ						$p = 3, n = 10$					
1.1	2	4	7	12	16	22	29	53	80	128	176
1.2	1	2	3	4	6	8	10	13	22	36	50
1.3	1	1	2	2	3	4	5	7	9	16	22
1.5	1	1	1	1	2	2	2	3	4	5	8
2.0	1	1	1	1	1	1	1	1	2	2	2
τ						$p = 5, n = 6$					
1.1	4	8	16	26	37	49	65	126	190	303	416
1.2	2	4	8	13	19	25	33	44	83	132	183
1.3	2	3	5	8	11	15	20	26	38	71	99
1.5	1	2	3	4	6	8	10	13	17	31	43
2.0	1	1	1	2	3	3	4	5	7	10	15
τ						$p = 5, n = 10$					
1.1	2	4	9	13	19	26	34	65	97	156	214
1.2	1	2	4	5	7	10	13	17	29	48	66
1.3	1	1	2	3	4	5	7	9	11	22	30
1.5	1	1	1	1	2	2	3	4	5	7	11
2.0	1	1	1	1	1	1	1	2	2	3	3
τ						$p = 8, n = 10$					
1.1	3	6	13	21	29	39	52	100	150	240	330
1.2	2	3	6	9	13	18	23	30	57	91	126
1.3	1	2	4	5	8	10	13	17	23	46	63
1.5	1	1	2	3	4	5	6	8	10	18	26
2.0	1	1	1	1	2	2	2	3	4	6	7
τ						$p = 8, n = 15$					
1.1	2	4	7	11	16	22	28	54	81	130	179
1.2	1	2	3	4	6	8	10	13	20	36	51
1.3	1	1	2	2	3	4	5	7	9	16	22
1.5	1	1	1	1	2	2	2	3	4	5	8
2.0	1	1	1	1	1	1	1	1	2	2	2

From Table 4, a notable difference is observed between its MRL_1 in Table 4 with its ARL_1 in Table 2 when τ is small. As an example, when p = 2, n = 5 and $\tau = 1.1$, the MRL_1 is 33 whereas the ARL_1 is 74.72, indicating that for more than half the time, the out-of-control condition is identified prior to the ARL_1, where the ARL_1 often falls within the 70th percentile. As the shift is typically detected before the ARL_1, evaluating the chart only based on the ARL_1 will inaccurately represent the chart's true performance. For larger values of τ, for example $\tau = 2.0$, the MRL_1 and ARL_1 become closer to each other, showing that their run length distribution is less skewed for large τ. As an example, for p = 2, n = 5 and $\tau = 2.0$, the MRL_1 is 2 whereas the ARL_1 is 2.10.

From Table 4, as τ, n and p increase, the differences between extreme percentiles decrease. For larger τ, n and p values, a smaller variation among its out-of-control run lengths is observed. For instance, the difference between its 5th and 95th percentile when p = 2, n = 5 and $\tau = 1.1$ is 274 (i.e., 277 – 3), while for p = 2, n = 5 and $\tau = 2.0$, the difference is only 4 (i.e., 5 – 1). Likewise, the corresponding difference between the extreme percentiles for p = 2, n = 10, and $\tau = 1.1$ is 161 as opposed to the difference of 274 for p = 2, n = 5, and $\tau = 1.1$.

From Tables 3 and 4, the in-control percentiles and out-of-control percentiles for small and moderate τ are skewed to the right, hence designing the chart with its *ARL* might not be the best approach. Hence, this chart is now designed with its *MRL*. For fair comparisons between the two designs, the ξ in Section 4.2 is equivalent to its MRL_0 in Table 3. For instance, for p = 2, n = 5 and $\tau = 1.1$, the MRL_0 = 207, hence $\xi = 207$. Table 5 presents the optimal charting parameters for the *MRL*-based design, along with their 5th percentile (Q_{05}), MRL_1, and 95th percentile (Q_{95}). As an example, for p = 2, n = 5 and $\tau = 1.1$, the optimal (*L, K*) = (25, 3.31), yielding (Q_{05}, MRL_1, Q_{95}) = (2, 25, 265).

By comparing Tables 2 and 5 for small τ, p and n, the L in Table 2 is typically larger than that from the *MRL*-based design (Table 5). As an example, when p = 2, n = 5 and $\tau = 1.1$, the optimal L from Table 2 is 47, but the optimal L from Table 5 is 25. The optimal K from Table 2 is also mostly larger than the optimal K from Table 5, suggesting a smaller conforming region. For instance, for p = 2, n = 5, and $\tau = 1.1$, the optimal K in Table 2 is 3.60, but the optimal K in Table 5 is 3.31.

Next, a comparison between the MRL_1 in Tables 4 and 5 shows that the MRL_1 from Table 5 is smaller than that from Table 4, especially when τ is small. As an example, when p = 5, n = 10 and $\tau = 1.1$, the MRL_1 in Table 4 is 26, whereas the MRL_1 in Table 5 is 20. Hence, the *MRL*-based design produces better MRL_1 performance, as both designs have the same MRL_0. The smaller MRL_1 translates to a smaller number of samples required for the detection of shifts.

The optimal (*L, K*) in Table 5 can only be determined if τ is known, which is not possible in several scenarios. Hence, the optimal (*L, K*) based on the *EMRL* is also presented. In this paper, a large range of $\left(\tau_{\min}, \tau_{\max}\right) = \left(1, 2\right]$ is adopted to account for the uncertainty in τ. The optimal (*L, K*), together with its associated expected 5th percentile (EQ_{05}), *EMRL* and expected 95th percentile (EQ_{95}), is shown in Table 6 for the same p and n values in Table 5.

From Table 6, the chart can be adopted even when τ could not be specified. For example, for p = 2 and n = 5, practitioners can select (*L, K*) = (14, 3.08) to operate the chart.

Table 5: Optimal charting parameters of the *MRL*-based design with their Q_{05}, MRL_1 and Q_{95}

τ	p = 2									
	$n = 5$					$n = 10$				
	L	K	Q_{05}	MRL_1	Q_{95}	L	K	Q_{05}	MRL_1	Q_{95}
1.1	25	3.31	2	25	265	15	2.24	2	15	158
1.2	11	2.96	1	10	98	6	2.01	1	5	47
1.3	5	2.62	1	5	52	8	2.59	1	3	19
1.5	10	2.95	1	3	18	1	1.56	1	1	11
2.0	4	2.54	1	1	6	11	2.19	1	1	2
τ	$p = 3$									
	$n = 5$					$n = 10$				
1.1	30	3.57	3	30	314	16	2.84	2	16	171
1.2	12	3.13	1	12	126	5	2.43	1	5	55
1.3	8	2.94	1	7	68	5	2.45	1	3	24
1.5	3	2.47	1	3	33	1	1.85	1	1	12
2.0	11	3.14	1	2	7	3	2.27	1	1	2
τ	$p = 5$									
	$n = 6$					$n = 10$				
1.1	37	4.03	3	37	390	20	3.02	2	20	207
1.2	17	3.57	2	17	181	8	2.68	1	7	69
1.3	10	3.26	1	10	106	7	2.63	1	4	31
1.5	5	2.86	1	5	53	9	2.75	1	2	9
2.0	2	2.33	1	2	23	7	2.66	1	1	3
τ	$p = 8$									
	$n = 10$					$n = 15$				
1.1	30	3.56	3	30	312	17	2.86	2	17	174
1.2	12	3.13	1	12	127	5	2.43	1	5	55
1.3	8	2.93	1	7	68	5	2.44	1	3	24
1.5	3	2.46	1	3	33	1	1.85	1	1	13
2.0	10	3.08	1	2	7	3	2.27	1	1	2

Table 6: Optimal charting parameters of the *EMRL*-based design with their EQ_{05}, *EMRL* and EQ_{95}

n	L	K	EQ_{05}	*EMRL*	EQ_{95}
	$p = 2$				
5	14	3.08	1.15	10.73	67.37
10	12	2.71	1.07	6.41	39.00
n	$p = 3$				
5	11	3.09	1.19	13.05	80.80
10	9	2.64	1.05	7.09	42.64
n	$p = 5$				
6	15	3.50	1.31	16.90	109.02
10	10	2.76	1.10	8.26	51.07
n	$p = 8$				
10	7	2.85	1.10	13.77	82.54
15	9	2.64	1.05	7.09	42.69

6. Real-Life Application

This section shows the implementation of the chart on an actual example from Giner-Bosch *et al*. (2019). From that example, an investment company intends to monitor their investment risk from $p = 3$ industrial sectors: S_1 (automotive), S_2 (aeronautic) and S_3 (electronic) for $n = 5$ regions: R_1 (Africa), R_2 (North America), R_3 (South America), R_4 (Asia) and R_5 (Europe). Table 7 shows the summary statistics ($\bar{\mathbf{X}}$, $\mathbf{S}$ and $\hat{\gamma}^2$) of the rate of returns for years

2000 to 2016. Readers are suggested to refer to Giner-Bosch *et al*. (2019) on the raw data of the actual rate of returns.

Table 7: Summary statistics ($\bar{\mathbf{X}}$, $\mathbf{S}$ and $\hat{\gamma}^2$) of the rate of returns for years 2000 to 2016

		$\bar{\mathbf{X}}$		$\mathbf{S}$		$\hat{\gamma}^2$
2000	S_1	19.82	9.33	1.35	0.12	0.0041
	S_2	40.14	1.35	7.22	1.17	
	S_3	9.78	0.12	1.17	2.41	
2001	S_1	20.64	3.72	3.65	0.04	0.0017
	S_2	38.14	3.65	8.75	4.14	
	S_3	10.78	0.04	4.14	3.28	
2002	S_1	20.00	4.70	-0.57	0.39	0.0005
	S_2	38.74	-0.57	1.05	-0.04	
	S_3	9.36	0.39	-0.04	1.35	
2003	S_1	19.78	1.52	0.58	0.46	0.0014
	S_2	40.56	0.58	3.07	0.63	
	S_3	10.3	0.46	0.63	0.23	
2004	S_1	19.66	1.22	1.29	-0.14	0.0020
	S_2	38.54	1.29	8.68	-2.03	
	S_3	10.38	-0.14	-2.03	2.61	
2005	S_1	19.30	2.58	3.39	-0.66	0.0015
	S_2	39.48	3.39	6.60	-0.20	
	S_3	9.56	-0.66	-0.20	0.60	
2006	S_1	19.26	1.13	-1.68	-0.54	0.0006
	S_2	40.16	-1.68	6.09	2.07	
	S_3	8.70	-0.54	2.07	2.21	
2007	S_1	20.22	4.28	3.65	3.87	0.0018
	S_2	39.00	3.65	7.27	3.99	
	S_3	9.28	3.87	3.99	4.09	
2008	S_1	19.94	1.59	1.06	1.31	0.0014
	S_2	40.42	1.06	7.82	4.26	
	S_3	9.18	1.31	4.26	3.79	
2009	S_1	19.66	4.81	1.91	0.20	0.0013
	S_2	39.50	1.91	3.32	-0.97	
	S_3	8.90	0.20	-0.97	1.94	
2010	S_1	8.22	1.17	-2.08	-2.44	0.0005
	S_2	20.32	-2.08	5.40	4.08	
	S_3	5.48	-2.44	4.08	5.75	
2011	S_1	11.98	4.38	-1.78	-0.56	0.0026
	S_2	20.42	-1.78	2.54	0.75	
	S_3	5.44	-0.56	0.75	0.53	
2012	S_1	9.78	2.41	2.28	-0.67	0.0079
	S_2	21.48	2.28	10.16	1.06	
	S_3	5.06	-0.67	1.06	0.94	
2013	S_1	8.96	3.12	-1.52	-1.88	0.0016
	S_2	20.24	-1.52	1.94	2.03	
	S_3	5.14	-1.88	2.03	3.64	
2014	S_1	10.80	4.76	-1.39	-0.43	0.0041
	S_2	18.20	-1.39	4.20	0.29	
	S_3	4.16	-0.43	0.29	0.23	
2015	S_1	10.84	1.55	0.66	0.71	0.0035
	S_2	19.10	0.66	2.91	1.84	
	S_3	5.08	0.71	1.84	1.76	
2016	S_1	8.26	5.00	-0.52	1.98	0.0062
	S_2	20.88	-0.52	7.25	1.88	
	S_3	5.34	1.98	1.88	1.61	

As the investment company intends to monitor investment risk, monitoring γ is a good choice as it links variability in returns ($\boldsymbol{\Sigma}$) with its expected return $\boldsymbol{\mu}$. From Giner-Bosch *et al*. (2019), years 2000 to 2009 shows satisfactory investment returns. Thus, they are the Phase I sample used to estimate $\hat{\gamma}_0$. From the average $\hat{\gamma}^2$ for this period, $\hat{\gamma}_0^2$ is estimated as 0.001638, i.e. $\hat{\gamma}_0 = 0.04047$. The years 2010 to 2016 are the Phase II data and the company would like to detect changes in the γ_0 compared to the Phase I period. Suppose the company is interested in detecting an increase of 10% in γ_0 . Thus, for this paper, τ is set as 1.1.

The multivariate side-sensitive synthetic γ chart is implemented through two approaches. In the first approach, the existing design based on the *ARL* is adopted, while the second approach is based on the *MRL*, as proposed in Section 4.2. In the first approach, the constraint for ARL_0 = 370.4, which results in (L, LCL, UCL)=(56,-0.002355,0.003993), with an ARL_1 of 87.92. However, adopting these charting parameters resulted in a MRL_0 of 202 and a MRL_1 of 39. This shows that false alarms frequently occur before the ARL_0 and shifts will also be frequently detected before the ARL_1. For the second approach based on the *MRL*, $(L, LCL, UCL) = (30, -0.002093, 0.003731)$, with a lower MRL_1 of 30. The width between the *LCL* and *UCL* is more narrow compared to the design based on the *ARL*, hence it is easier for a sample to be defined as a non-conforming sample. Figure 2 shows the monitoring of $\hat{\gamma}^2$ for the Phase II data, where Figure 2 (a) is based on the *ARL* while Figure 2 (b) is based on the *MRL*.

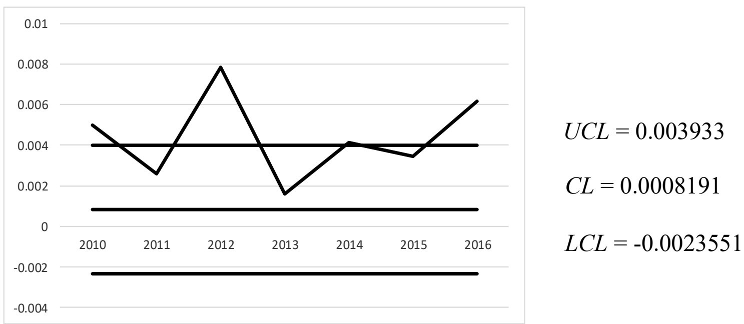

(a) *ARL*-based design

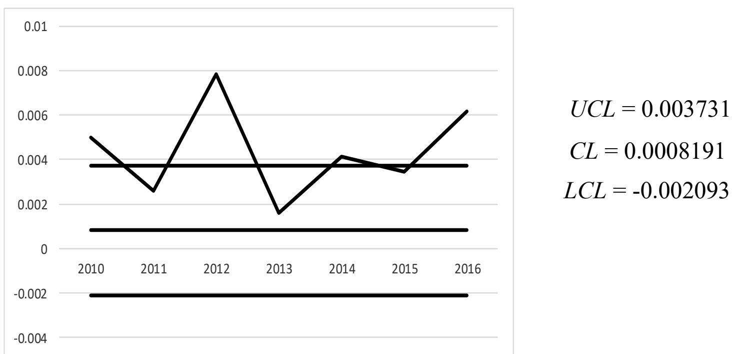

(b) *MRL*-based design

Figure 2: Monitoring Phase-II data through the multivariate side-sensitive synthetic γ chart for known τ

From Figures 2 (a) and (b), the years 2012, 2014 and 2016 are detected as non-conforming samples, with $CRL_1 = 3$, $CRL_2 = 2$ and $CRL_3 = 2$. As all the CRLs are less than the L of 56 and L of 30 for the *ARL*-based and *MRL*-based designs, respectively, these samples are detected as out-of-control samples for both designs. Note that although for this particular example both designs detected the same out-of-control samples, the width of the conforming region for the *MRL*-based design is more narrow, hence for $0.003731 < \hat{\gamma}^2 < 0.003993$, the *MRL*-based defines the sample as non-conforming whereas the *ARL*-based design defines that sample as conforming, resulting in a possible quicker detection. Furthermore, the *MRL*-based design gives a more accurate representation of the chart's actual performance, as shown in the significant difference between its ARL_0 and MRL_0, as well as its ARL_1 and MRL_1.

MRL-based designs requires τ to be specified. Hence, this paper also illustrates the *EMRL*-based design, with (τmax_{min}=1,2), where $(L, LCL, UCL) = (11, -0.001711, 0.003349)$. For comparison, (L,LCL,UCL) = (30,-0.002125, 0.003764) for the design based on the expected *ARL* (*EARL*). Figure 3 shows the monitoring of $\hat{\gamma}^2$ for unknown τ, where Figure 3 (a) is based on the *EARL* while Figure 3 (b) is based on the *EMRL*.

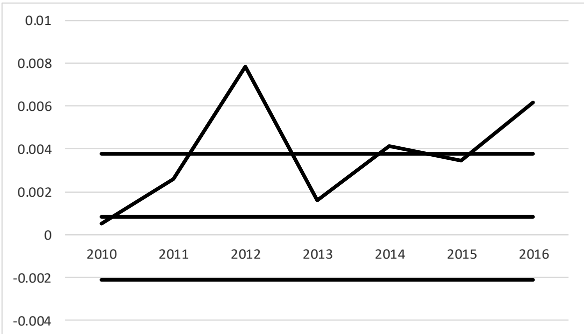

UCL = 0.003764

CL = 0.0008191

LCL = -0.002125

(a) *EARL*-based design

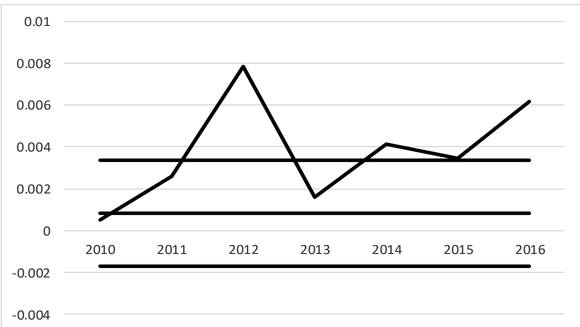

UCL = 0.003349

CL = 0.0008191

LCL = -0.001711

(b) *EMRL*-based design

Figure 3: Monitoring Phase-II data through the multivariate side-sensitive synthetic γ chart for unknown τ

Similar with Figure 2, the *EARL*-based design in Figure 3 (a) shows the years 2012, 2014 and 2016 as non-conforming samples, with CRL_1, CRL_2 and CRL_3 of 3, 2 and 2, respectively. Since all the CRLs are less than the L of 30, these samples are out-of-control. For the *EMRL*-based design in Figure 3 (b), the years 2012, 2014, 2015 and 2016 are detected as non-conforming samples, with CRL_1, CRL_2, CRL_3 and CRL_4 of 3, 2, 1 and 1, respectively. As all the CRLs are less than the L of 11, these samples are out-of-control. Hence, by comparison with the *EARL*-based design, the *EMRL*-based design detected more out-of-control samples.

7. Conclusion

This paper aims to achieve two objectives. Firstly, the paper studies the run length distribution of the existing *ARL*-based design for the multivariate side-sensitive synthetic γ chart. Secondly, the chart's design based on its *MRL* and *EMRL* are proposed. From the run length distribution, its MRL_0 is significantly smaller than its ARL_0, indicating that false alarms usually occur prior to its ARL_0, resulting in a lack of confidence towards the chart if interpretations on the chart's performance is based solely on its ARL_0. Furthermore, the MRL_1 for small shift sizes is also smaller than the ARL_1. Hence, its in-control run lengths and out-of-control run lengths for small shifts are right-skewed, making the *MRL* a better performance indicator. From the *MRL*-based design, their optimal charting parameters resulted in a smaller MRL_1. Hence, practitioners adopting the charting parameters proposed in this paper will reduce the number of samples needed for the detection of out-of-control conditions, resulting in faster corrective action being taken. Furthermore, this paper also proposed the design of the chart through the *EMRL* for practitioners who could not estimate the exact value of τ .

A main limitation of this study is the normality assumption in the designs proposed. As the distributional properties of $\hat{\gamma}$ for non-normal data is not available in the existing literature, designs for non-normal data could not be proposed. Hence, future research could focus on deriving the distributional properties of $\hat{\gamma}$ for non-normal data and subsequently propose designs for non-normal data. Another limitation of this study is it is focused only on the multivariate side-sensitive synthetic γ chart. Future studies can study the run length distribution of other charts.

References

Abbasi S.A. & Adegoke N.A. 2018. Multivariate coefficient of variation control charts in phase I of SPC. *The International Journal of Advanced Manufacturing Technology*. **99**: 1903-1916.

Adegoke N.A., Dawod A., Adeoti O.A., Sanusi R. A. & Abbasi, S. A. 2022. Monitoring multivariate coefficient of variation for high-dimensional processes. *Quality and Reliability Engineering International* **38**(5): 2606-2621.

Ayyoub H.N., Khoo M.B., Saha S. & Castagliola P. 2020. Multivariate coefficient of variation charts with measurement errors. *Computers & Industrial Engineering* **147**: 106633.

Castagliola P., Celano G. & Psarakis S. 2011. Monitoring the coefficient of variation using EWMA charts. *Journal of Quality Technology*. **43**(3): 249 – 265.

Chew X.Y., Khoo M.B.C., Khaw K.W., Yeong W.C. & Chong Z.L. 2019. A proposed variable parameter control chart for monitoring the multivariate coefficient of variation. *Quality and Reliability Engineering International* **35**(7): 2442-2461.

Chew X.Y., Khaw K.W. & Yeong W.C. 2020. The efficiency of run rules schemes for the multivariate coefficient of variation: a Markov chain approach. *Journal of Applied Statistics* **47**(3): 460-480.

Chew X.Y., Khaw K.W. & Lee M.H. 2022. The efficiency of run rules schemes for the multivariate coefficient of variation in short runs process. *Communications in Statistics-Simulation and Computation* **51**(6): 2942-2962.

Giner-Bosch V., Tran K.P., Castagliola P. & Khoo M.B.C. 2019. An EWMA control chart for the multivariate coefficient of variation. *Quality and Reliability Engineering International*. **35**(6): 1515-1541.

Haq A. & Khoo M.B.C 2022. Monitoring multivariate coefficient of variation with individual observations. *Quality and Reliability Engineering International* **38**(8): 4236-4246.

Hu X.L., Zhang S.Y., Zhang J. & Saghir A. 2023. Efficient CUSUM control charts for monitoring the multivariate coefficient of variation. *Computers & Industrial Engineering* **179**: 109159.

Jalilibal Z., Amiri A, Castagliola P. & Khoo M.B.C. 2021. Monitoring the coefficient of variation: A literature review. *Computers & Industrial Engineering* **161**: 107600.

Karimi H., Khaw K.W, Chew X.Y., Chong Z.L. & Lim S.T. 2023. Variable sample size control charts for monitoring the multivariate coefficient of variation based on median run length and expected median run length. *Journal of Science and Technology* **15**(2): 54-80.

Khatun M., Khoo M.B.C., Lee M.H. & Castagliola P. 2018. One-sided control charts for monitoring the multivariate coefficient of variation in short production runs. *Transactions of the Institute of Measurement and Control* **41**(6): 1712-1728.

Khaw K.W., Khoo M.B.C., Castagliola P. & Rahim M.A. 2018. New adaptive control charts for monitoring the multivariate coefficient of variation. *Computers & Industrial Engineering* **126**: 595-610.

Khaw K.W., Chew X.Y., Yeong W.C. & Lim S.L. 2019. Optimal design of the synthetic control chart for monitoring the multivariate coefficient of variation. *Chemometrics and Intelligent Laboratory Systems* **186**: 33-40.

Lee M.H., Lim V.Y.C., Chew X.Y., Lau M.F., Yakub S. & Then P.H.H. 2020. Design of the synthetic multivariate coefficient of variation based on the median run length. *Advances in Mathematics: Scientific Journal* **9**(9): 7397-7406.

Lim A.J.X., Khoo M.B.C., Teoh W.L. & Haq A. 2017. Run sum chart for monitoring multivariate coefficient of variation. *Computers & Industrial Engineering* **109**: 84-95.

Lim S.L., Yeong W.C., Khoo M.B.C., Chong Z.L. & Khaw K.W. 2019. An alternative design for the variable sample size coefficient of variation based on the median run length and expected median run length. *International Journal of Industrial Engineering* **26**(2): 199-220.

Sabahno H. & Celano G. 2023. Monitoring the multivariate coefficient of variation in presence of autocorrelation with variable parameters control charts. *Quality Technology & Quantitative Management* **20**(2): 184-210.

Teoh W.L., Lim J.Y., Khoo M.B.C., Chong Z.L. & Yeong W.C. 2019. Optimal designs of EWMA charts for monitoring the coefficient of variation based on median run length and expected median run length. *Journal of Testing and Evaluation* **47**(1): 459-479.

Yeong W.C., Khoo M.B.C, Teoh W.L. & Castagliola P. 2016. A control chart for the multivariate coefficient of variation. *Quality and Reliability Engineering International* **32**(3): 1213-1225.

Yeong W.C., Lim S.L., Khoo M.B.C., Khaw K.W. & Ng P.S. 2021a. An optimal design of the synthetic coefficient of variation chart based on the median run length. *International Journal of Reliability, Quality and Safety Engineering* **28**(3): 2150018.

Yeong W.C., Lee P.Y., Lim S.L., Ng P.S. & Khaw K.W. 2021b. Optimal designs of the side sensitive synthetic chart for the coefficient of variation based on the median run length and expected median run length. *PloS One* **16**(7): e0255366.

Yeong W.C., Lim S.L., Chong Z.L., Khoo M.B.C. & Saha S. 2022. A side-sensitive synthetic chart for the multivariate coefficient of variation. *PloS One* **17**(7): e0270151.

Centre for Big Data and Blockchain Technologies
CoE for Advanced Cloud
Multimedia University
63100 Cyberjaya
Selangor, MALAYSIA
*E-mail: wcyeong@mmu.edu.my**

School of Accounting and Finance
Faculty of Business & Law
Taylor's University
47500 Subang Jaya
Selangor, MALAYSIA
E-mail: sokli.lim@taylors.edu.my, ulshuhadashamsun.nur@sd.taylors.edu.my

Department of Electronic Engineering
Faculty of Engineering and Green Technology
Universiti Tunku Abdul Rahman
31900 Kampar
Perak, MALAYSIA
E-mail: chongzl@utar.edu.my

Department of Physical and Mathematical Science
Faculty of Science
Universiti Tunku Abdul Rahman
31900 Kampar
Perak DR, MALAYSIA
E-mail: psng@utar.edu.my

Received: 18 October 2025
Accepted: 19 December 2025

*Corresponding author